Title

Long-Range Order in Nanocrystal Assemblies Determines Charge Transport of Films

Journal

ACS Omega, 2(7)

ISSN

2470-1343

Authors

Sainato, Michela

Shevitski, Brian

Sahu, Ayaskanta

et al.

Publication Date

2017-07-31

DOI

10.1021/acsomega.7b00433

Peer reviewed

ACS OMEGA

Article

http://pubs.acs.org/journal/acsodf

Long-Range Order in Nanocrystal Assemblies Determines Charge Transport of Films

Michela Sainato,[†,§] Brian Shevitski,[‡] Ayaskanta Sahu,[‡,∥] Jason D. Forster,[‡] Shaul Aloni,[‡] Giuseppe Barillaro,*[,†] and Jeffrey J. Urban*[,‡]

[†]Dipartimento di Ingegneria dell'Informazione, Università di Pisa, Via G. Caruso 16, 56111 Pisa, Italy

[‡]Molecular Foundry, Lawrence Berkeley National Laboratory, 67 Cyclotron Road, 94720 Berkeley, United States

Supporting Information

ABSTRACT: Self-assembly of semiconductor nanocrystals (NCs) into two-dimensional patterns or three-dimensional (2-3D) superstructures has emerged as a promising low-cost route to generate thin-film transistors and solar cells with superior charge transport because of enhanced electronic coupling between the NCs. Here, we show that lead sulfide (PbS) NCs solids featuring either short-range (disordered glassy solids, GSs) or long-range (superlattices, SLs) packing order are obtained solely by controlling deposition conditions of colloidal solution of NCs. In this study, we demonstrate the use of the evaporation-driven self-assembly method results in PbS NC SL structures that are observed over an area of 1 mm × 100 μm, with long-range translational order of up to 100 nm. A number of ordered domains appear to have nucleated simultaneously and grown together over the whole area, imparting a polycrystalline texture to the 3D SL films. By contrast, a conventional, optimized spin-coating deposition method results in PbS NC glassy films with no translational symmetry and much shorter-range packing order in agreement with state-of-the-art reports. Further, we investigate the electronic properties of both SL and GS films, using a field-effect transistor configuration as a test platform. The long-range ordering of the PbS NCs into SLs leads to semiconducting NC-based solids, the mobility (μ) of which is 3 orders of magnitude higher than that of the disordered GSs. Moreover, although spin-cast GSs of PbS NCs have weak ambipolar behavior with limited gate tunability, SLs of PbS NCs show a clear p-type behavior with significantly higher conductivities.

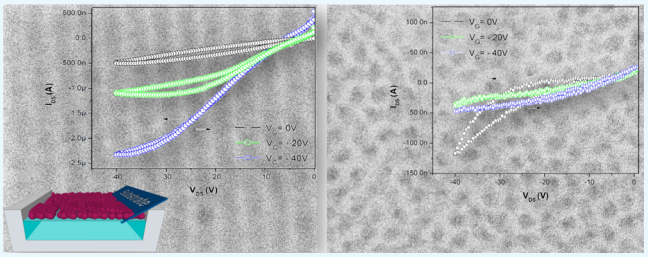

INTRODUCTION

Semiconductor nanocrystals (NCs) display strong size-dependent optical and electronic properties due to the quantum confinement of the electronic wavefunctions.[1,2] Recent advances in synthetic approaches for semiconductor NCs have enabled atomic-scale control of composition, size, size dispersion, shape, and crystal structure of the resulting colloids.[3,4] The use of short-chain ligands, molecular solders,[5−8] and post-thermal or chemical treatments of NC solids has enabled improved charge transport through NC films. However, all of the aforementioned methods drastically change the surface chemistry of the final NC solids.

Although improvements in inter-NCs coupling are exciting, the ability to prepare self-assembled NC superstructures over large areas (wafer scale) by controlling the formation of two-dimensional (2D) and three-dimensional (3D) networks with a high degree of order is still low.[9,10] In fact, the formation of periodicity with long-range ordering in self-assembled NC superstructures has been limited by fast dewetting of a volatile solvent and polarity of the solvent. Therefore, the ability to preserve the periodicity as well as long-range crystalline order over a large scale is one of the key challenges preventing the application of 2D or 3D NC solids for low-cost production of nanoelectronics by roll-to-roll fabrication.

In this scenario, the NC superlattice (SL) assembly can be leveraged to combine the advantages of tunable quantum-confined energy levels provided by quantum dots with enhanced charge transport due to the improved electronic coupling between NCs, thus leading to improved performance. However, although theoretical models have been proposed to investigate the effects of ordering on the electronic transport in semiconductor NC assemblies, experimental results on the effect of structural order on electronic properties are still a challenge.[11−13]

PbS NCs are one of the most extensively investigated systems for several applications, including solar cells, photodetectors, and light-emitting devices in the near-infrared (NIR) region because of their tunable synthesis, optimal band gap range, and high optical absorption.[14,15] In spite of their interesting optoelectronic properties, PbS NCs have rarely been used for transistor-based devices because of their extremely low charge carrier mobilities in thin films.[16,17] The main reason for this is the difficulty of controlling the arrangement of PbS NCs in a solid film at both nano-[18] and macro-scales.[19]

Received: April 10, 2017
Accepted: June 14, 2017
Published: July 18, 2017

DOI: 10.1021/acsomega.7b00433
ACS Omega 2017, 2, 3681−3690

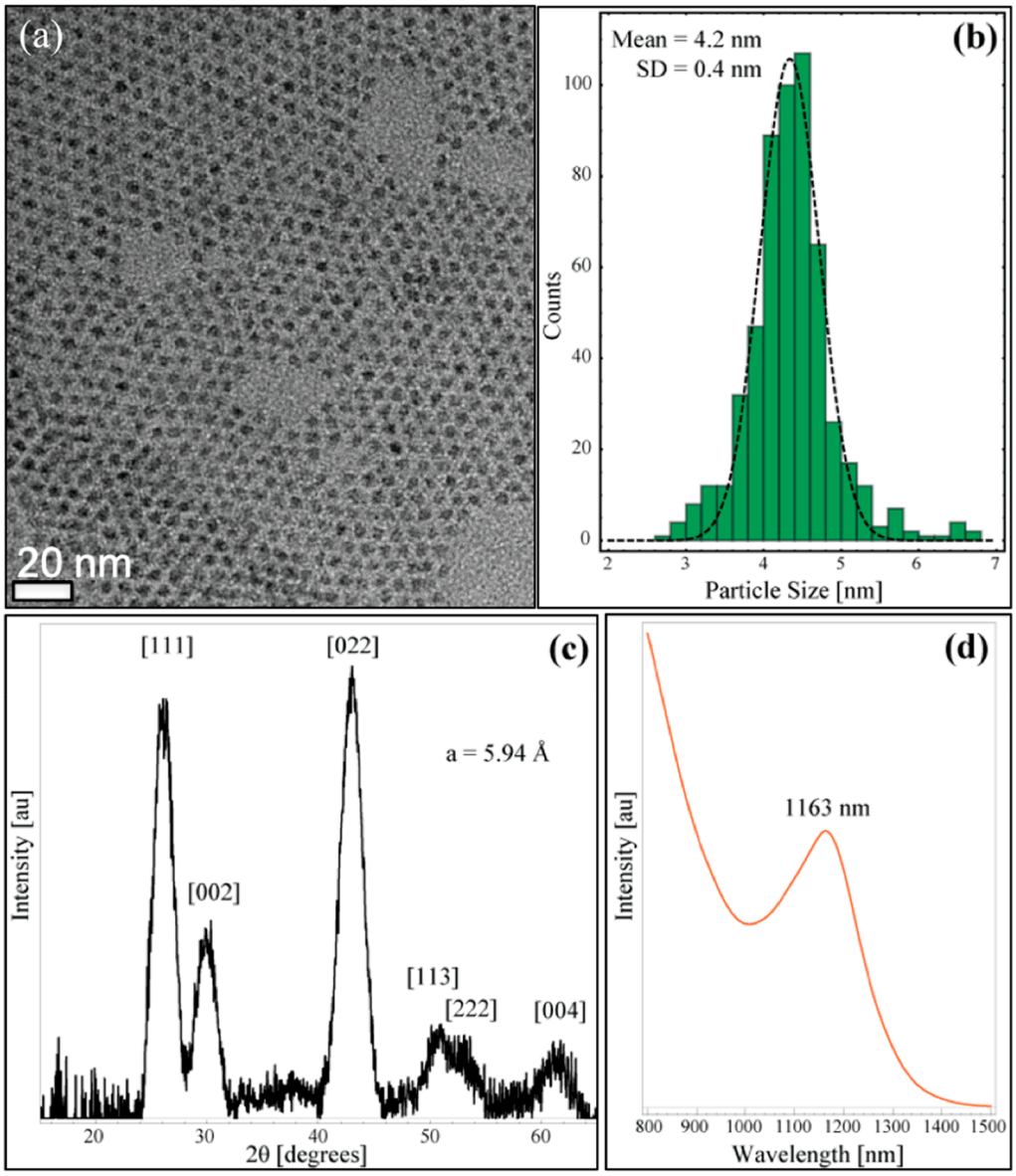

Figure 1. Synthesis and characterization of PbS NCs. (a) TEM image of the as-synthesized PbS NCs. (b) Size distribution histogram obtained by sampling ~500 nanoparticles, resulting in a nominal particle size of 4.2 nm. (c) XRD pattern demonstrating that the NCs have an fcc crystal structure, with a lattice parameter of 5.94 Å. The widths of the peaks indicate a mean crystallite size of ~4 nm, according to the Debye–Scherrer formula. (d) UV–vis–NIR spectrum, with a distinct excitonic peak at 1163 nm.

In this study, we control the assembly of PbS over multiple length scales, from short to long range, and demonstrate that the extent of ordering can be a dominant factor for efficient charge transport in NC films. The evaporation-driven self-assembly of PbS NCs results in SL structures with an area greater than 1 mm × 100 μm. The SLs have ordered domains, which appear to have nucleated and grown together to cover the whole area, imparting a polycrystalline texture to 3D SL films. Conversely, conventional spin-coating deposition of PbS NCs leads to glassy solids (GSs) with a much shorter range of packing order and no long-range translational order. We investigate the electronic properties of both GS and SL films using a field-effect transistor (FET) configuration as a testing platform. Our results highlight that the long-range ordering arising from the close-packed arrangement of PbS NCs into SLs leads to semiconducting NC-based solids with a charge carrier mobility up to 3 orders of magnitude higher than that of disordered GSs. Further, GS films of PbS NCs show a weak ambipolar behavior with limited gate tunability, whereas SL films of PbS NCs show a p-type behavior with significantly higher conductivities, thus providing experimental evidence of the effect of the extent of packing order on the electrical properties of an NC semiconductor solid.

RESULTS AND DISCUSSION

Synthesis and Structural Characterization of PbS NCs.

Hot-injection synthesis is used to prepare 4.2 nm PbS NCs with spherical shape and size distribution of 11%, according to a previously described protocol.[20] Briefly, the synthesis is carried out using a lead oleate (PbOA) precursor mixed with lead(II) oxide (PbO) and oleic acid (OA) in 1-octadecene (ODE). A solution of bis(trimethylsilyl) sulfide in ODE is injected into the mixture at 100 °C under nitrogen to induce nucleation and growth of PbS NCs, thereby ultimately forming a stable colloidal suspension.[3,21,22]

DOI: 10.1021/acsomega.7b00433
ACS Omega 2017, 2, 3681–3690

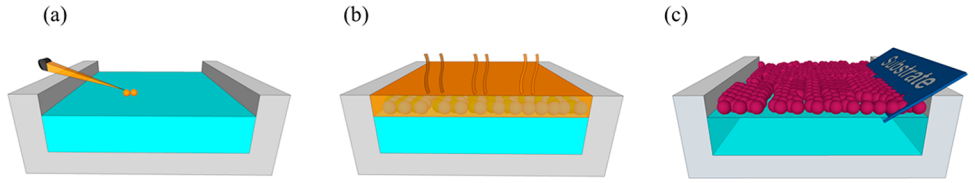

Figure 2. Schematic of the growth of an SL membrane by evaporation-mediated self-assembly of NCs on an immiscible liquid surface, using ACN and NCs in octane solution. (a) A small volume of NCs in octane is drop-cast on top of the ACN surface. (b) The growth of 3D SLs is induced by evaporation of octane, yielding a final membrane supported by the subphase after ∼10 min. The membrane keeps growing and sliding unidirectionally until the evaporation of octane is complete. (c) The resulting free-standing NC membrane can be transferred from the subphase surface to any substrate by "scooping" it up.

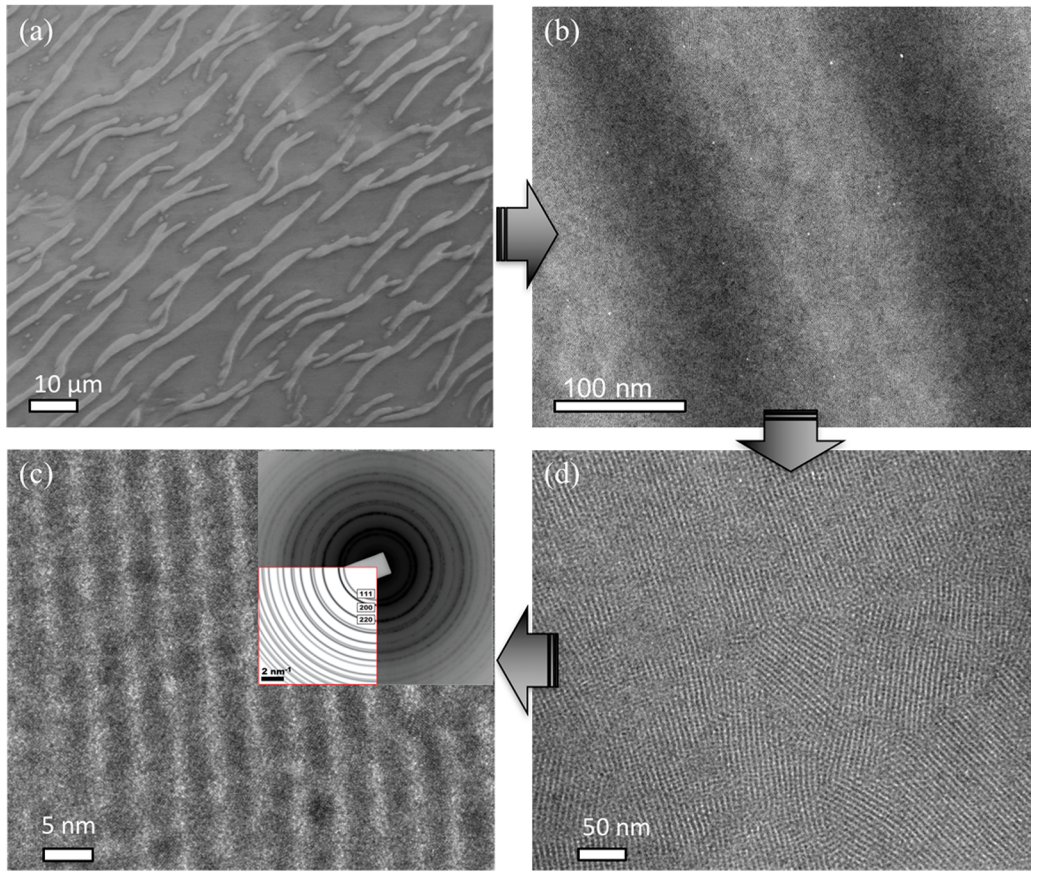

Figure 3. Morphological analysis of PbS SL membrane. (a) SEM image of SL membranes of 4 nm PbS NCs transferred on top of SiO_2/Si wafer substrates. (b) TEM image showing the effect of thermocapillary convective flows resulting in an elongated macrostructure of PbS NCs. (c) TEM image of typical PbS SL membranes. The PbS NCs cocrystallize into SLs with relatively large grain sizes (∼100 nm), with different growth directions or lattice plane projections, as evidenced by the grain boundaries between adjacent domains. (d) TEM image of an SL with a clear periodicity of 5.7 nm. The inset is the selected-area electron diffraction (SAED) pattern showing that the individual quantum dots forming the SL have the same crystallographic structure as bulk PbS (fcc, a = 5.8 Å) and no preferred crystallographic orientation with respect to one another, evidenced by the rings in the diffraction pattern as opposed to individual Bragg reflection spots.

Quantitative structural and chemical analyses of the as-synthesized PbS NCs are performed with transmission electron microscopy (TEM), UV−vis spectroscopy, and X-ray diffraction (XRD), the results of which are summarized in Figure 1. A growth time of 5 min results in uniform, nearly spherical PbS NCs, as shown in the TEM image in Figure 1a. The size distribution histogram (Figure 1b) reveals a mean particle size of 4.2 nm with a standard deviation of 0.4 nm. The crystal structure and average crystallite size were confirmed by XRD, as shown in Figure 1c. The as-synthesized PbS NCs have a lattice constant of 5.94 Å and a face-centered cubic (fcc) crystal structure similar to that of bulk PbS. The absorbance spectrum (Figure 1d) shows the presence of an excitonic peak at ∼1.066 eV (1163 nm), indicating that the as-synthesized PbS quantum dots demonstrate quantum confinement because bulk PbS has a band gap (measured at the band edge) of ∼0.41 eV (3024 nm). By correlating the position of the first exciton peak in the absorbance spectra with the mean NC diameter (d_{NC}), we were able to determine d_{NC} optically, avoiding a lengthy TEM analysis for each synthesis run.[23]

Preparation and Characterization of PbS NC SL Membranes and Disordered Glassy Films. Lithography-free approaches to control the arrangement of NCs over large length scales for electrical devices are in high demand. Ordered arrangement of NCs enhances interparticle coupling, resulting in bandlike transport, which in turn results in devices with

DOI: 10.1021/acsomega.7b00433
ACS Omega 2017, 2, 3681−3690

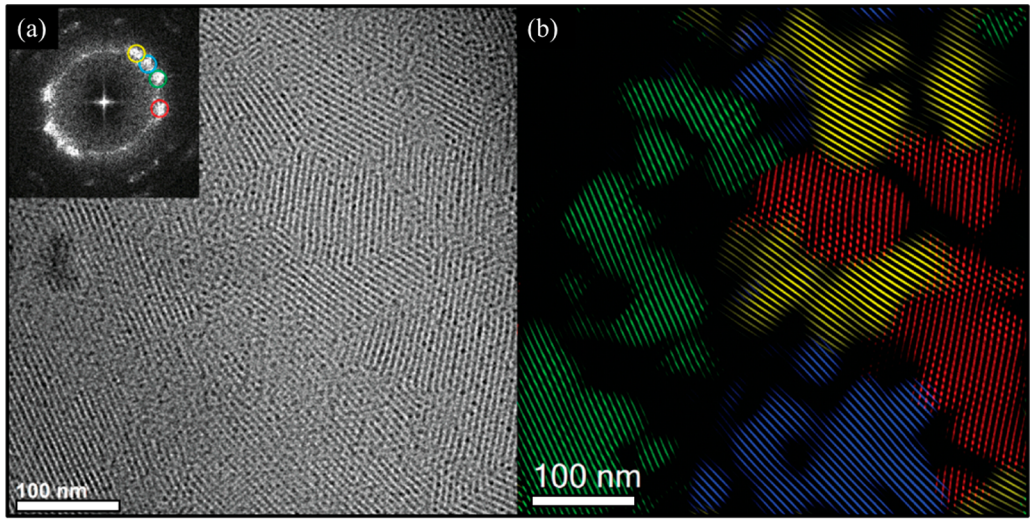

Figure 4. Morphological analysis of PbS SL membranes. (a) TEM image of a typical PbS SL membrane (inset: FFT). (b) False-color composite image of (a) made by masking the colored circles in the FFT. The false-color image illustrates the typical domain size of ∼100 nm observed in the SL membranes.

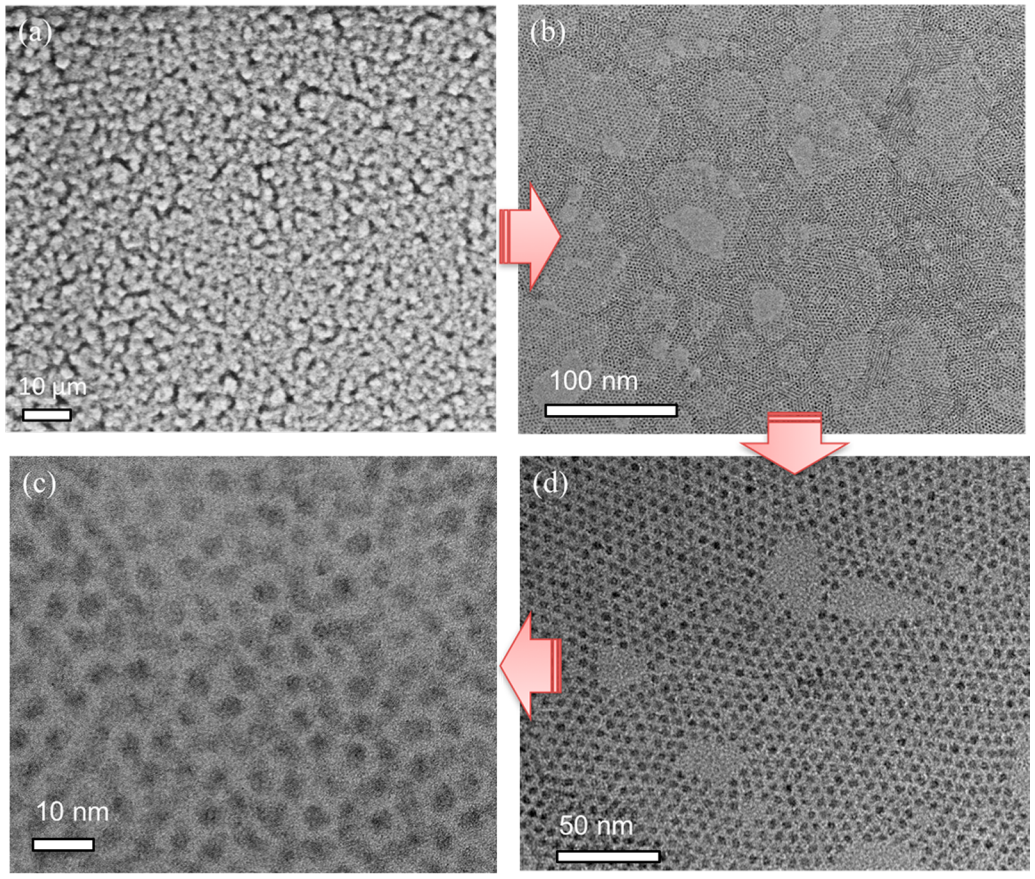

Figure 5. Morphological analysis of PbS spin-cast solids. (a) SEM image of spin-cast solids of 4 nm PbS NCs on top of SiO_2/Si wafer substrates. The scale bar is 10 μm. (b–d) TEM images of a typical PbS glassy thin film, obtained by spin-coating NCs from colloidal solutions onto 20 nm silicon nitride TEM windows.

enhanced electrical performance. Liquid–air interfacial assembly techniques, such as the Langmuir–Blodgett (LB) method, are widely employed to prepare ordered NC monolayers.[24] However, monolayers of small NCs with long-range order are difficult to obtain with the LB method, limiting its suitability for large-scale device applications.[25] In the last few years, significant efforts have concentrated on generating SL membranes and thin-film solids (TFs) from various colloidal NC systems.[26−28]

Evaporation-driven self-assembly of NCs on the surface of a polar organic subphase at room temperature (RT) results in 3D SL membranes with long-range translational order of up to 100 nm.[29,30] The fabrication method is depicted in Figure 2. First, 150 μL of 50 mg/mL PbS NCs in octane is drop-cast on the

DOI: 10.1021/acsomega.7b00433
ACS Omega 2017, 2, 3681−3690

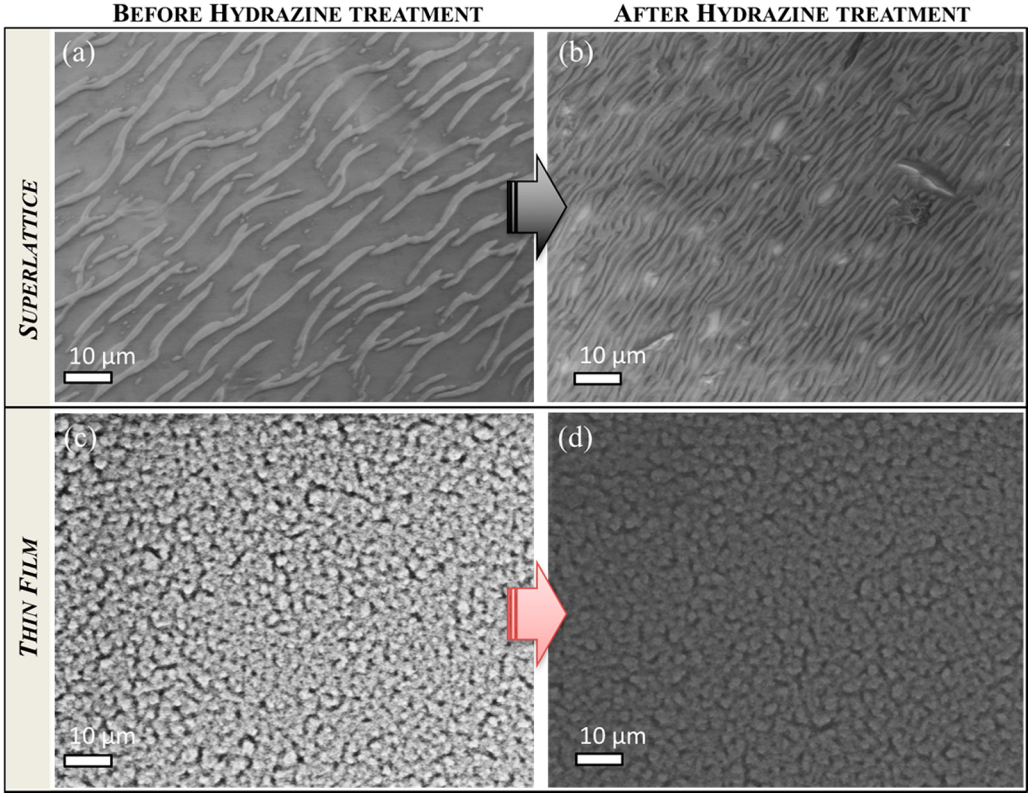

Figure 6. Preparation and characterization of PbS SL membranes and PbS spin-cast solids on SiO_2/Si wafer (~1 cm × 1 cm). SEM images of (a, b) SL membranes and (c, d) spin-cast solids of PbS NCs transferred on top of SiO_2/Si wafer substrates (a, c) before and (b, d) after 1 M hydrazine treatment for 4 h, so as to investigate the influence of the ligand exchange treatment on the uniformity and homogeneity of the final NC solids.

surface of acetonitrile (ACN) in a ~2 × 2 cm Teflon well (Figure 2a). The growth of SLs is driven by an evaporation-mediated self-assembly process (Figure 2b), yielding a membrane supported on the surface of the polar organic subphase after the complete evaporation of octane (~10 min), as shown in Figure 2b. This liquid-supported membrane can be readily scooped up and transferred to TEM grids or SiO_2/Si wafers for characterization (Figure 2c). Held together by van der Waals forces, the PbS NCs cocrystallize into SLs.

Figure 3 shows scanning electron microscopy (SEM) and TEM images of the as-synthesized PbS SL membrane at different magnifications. Figure 3a shows an SEM image of a 100 μm × 100 μm area of SiO_2/Si substrate (1 cm × 1 cm) coated with an as-synthesized SL layer consisting of 4.2 nm PbS NCs. The formation of SLs is strongly affected by the solvent evaporation process (Figure 2), which depends on several factors, such as fluctuations in solvent density and nanoparticle diffusion.[31,40]

Moreover, the evaporation rate of high-boiling-point solvents can dramatically affect the dimensionality of SLs. Changing the evaporation rate can lead to either 2D or 3D SL formation using the same NCs.[8] In our procedure, octane replaces commonly used high-boiling-point solvents such as tetrachloroethylene (TCE), allowing the assembly process to be completed in several minutes.[32,33] Convection driven by solvent evaporation in addition to electrostatic and van der Waals interactions modifies the particle assembly process. As reported in the literature, the origins of micron-scale structures of locally ordered assemblies of NCs are related to both the solvent evaporation rate and subphase viscosity.[34,35] Those macroscale structures formed in our SL membranes are shown in Figure 3a. We believe that thermocapillary convective flows engendered within an evaporating particle suspension give rise to the elongated micron-scale structures of PbS, as shown in Figure 3a.

In general, we observe uniform as-synthesized SL membranes of PbS NCs covering areas up to 1 × 1 mm^2, demonstrating the high quality of the drying-mediated, self-assembled SLs. Low-magnification TEM imaging (Figure 3b,d) shows the long-range order of the 3D SL of PbS NCs. In this image, a number of ordered domains appear to have nucleated simultaneously and grown together, imparting a polycrystalline texture to the 3D SL. Figure 3d shows an SL with a clear periodicity of 5.7 nm. The SAED pattern (Figure 3d, inset) shows that individual NCs have the same atomic crystallographic structure as bulk PbS (fcc, a = 5.8 Å) and no preferred atomic crystallographic orientation with respect to one another, as evidenced by the rings in the diffraction pattern as opposed to individual Bragg reflection spots. Orientations were determined by fast Fourier transforms (FFTs) of the TEM images in Figure S1. The FFT of the image in Figure S1a (inset) shows that in the PbS SL structure there is a preferred orientation of the crystal domains, which corresponds to the brightest spots in the FFT. A quantitative structural characterization of the extent of ordered packing of the SL films is reported in Figure 4. The FFT in the inset of Figure 4a shows domains of different crystallographic orientations of NCs in a 500 × 500 nm^2 area of an SL membrane. The false-color image in Figure 4b illustrates the typical domain size of ~100 nm observed in the SL membranes.

Electron microscopy (both SEM and TEM) characterization is also performed on PbS films, which have been spin-cast onto SiO_2/Si substrates (1 cm × 1 cm). Figure 5a shows the SEM image (100 μm × 100 μm) of a PbS film obtained via a layer-by-layer (LbL) sequential spin-coating technique. The LbL spin-

DOI: 10.1021/acsomega.7b00433
ACS Omega 2017, 2, 3681−3690

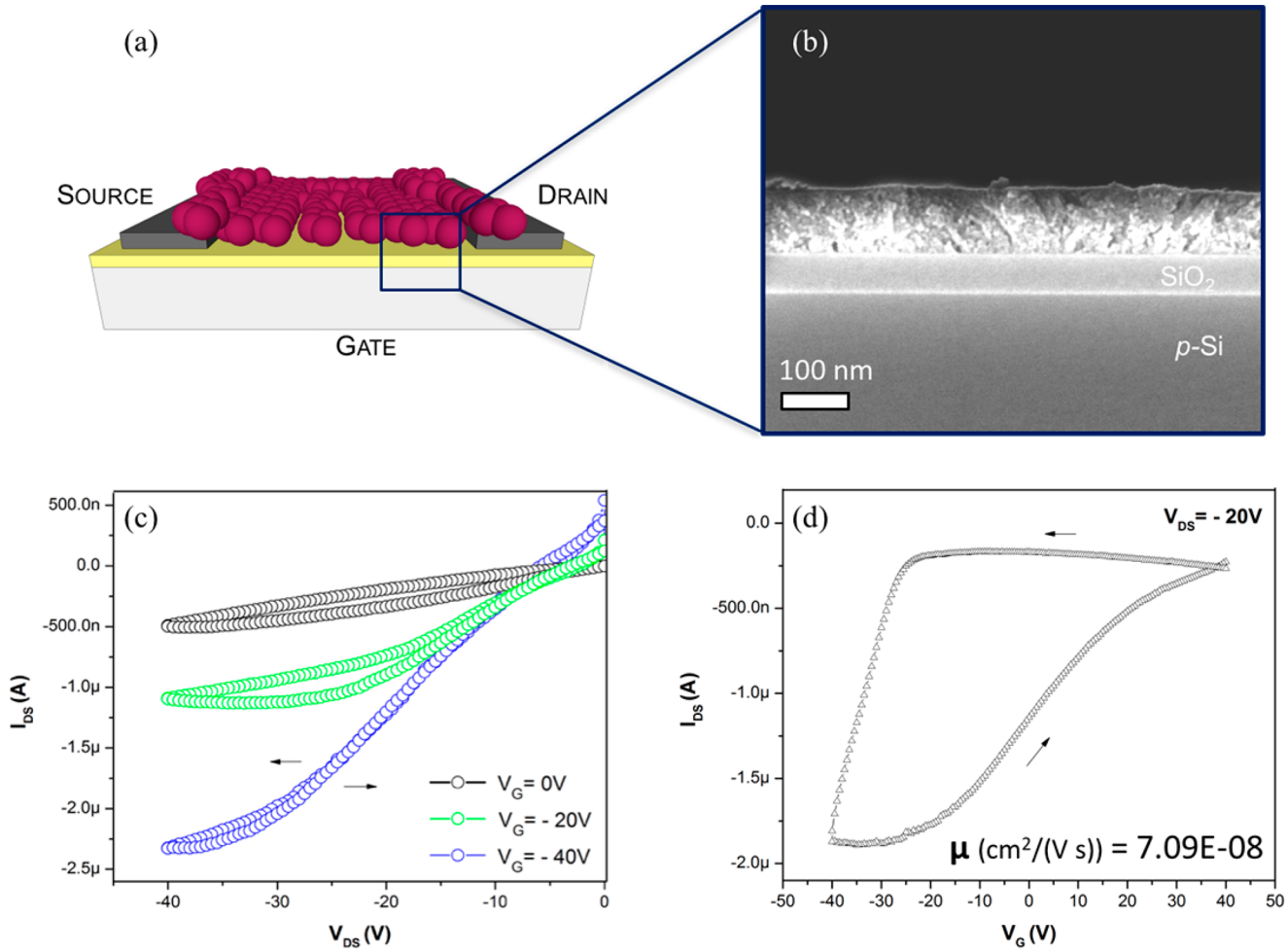

Figure 7. Electrical characterization of PbS SL solids. (a) Schematic cross section of an FET device using self-assembled NCs as a conduction channel. (b) SEM image of a PbS SL-FET cross section after hydrazine treatment. (c) Drain−source $I-V$ curves obtained at different gate voltages from a device using a PbS SL conduction channel (width and length of the channels were 1 mm and 100 μm, respectively). (d) Transfer curve with a fixed drain−source voltage of −20 V.

coating process is employed to improve the surface coverage of the film. It is well known that the thickness of the final film depends on the thickness of the dispersion layer on the substrate surface at the final rotation speed; this value is influenced by the viscosity and surface tension of the NC solution.[36] Because there is a surface tension gradient in the NC solution during the spin-coating process, the final coating gives rise to an incomplete surface coverage, forming PbS NC clusters that are similar in density and size but leaving sections of the substrate surface free of PbS NCs (Figure 5a). A low-magnification TEM image of a PbS NC solid after a single spin-coating step at RT is shown in Figure 5b. The film is spin-cast on top of an electron-transparent 20 nm silicon nitride TEM window mounted on a 2.12 mm silicon chip. Higher-magnification TEM images (Figure 5c) show uniformity in the size and shape of the NCs. We observe that by spin-coating NCs on a silicon nitride substrate short-range order is partially preserved but long-range translational order is not present (Figure 5c,d) and the NCs tend to cluster in small close-packed domains (Figure 5d). The orientations of NCs in these PbS thin films were determined by using FFTs of the TEM images, such as the one in Figure S1b. The FFT image (Figure S1b, inset) shows that no preferred crystallographic orientation exists in the PbS thin film, with disordered NC subphases leading to a "glassy" thin film, that possess short-range order but lacks long-range translational order (Figure 5), thus limiting its applicability for device applications.

Postdeposition chemical activation of both SL and GS films is carried out through hydrazine (N_2H_4) treatment,[35,11] with the aim of investigating the effect of a 4 h hydrazine treatment on both uniformity and homogeneity on the NC solids (Figure 6). Figure 6a shows the SEM image of a 100 μm × 100 μm area of a typical as-deposited SL layer. The SEM image in Figure 6b shows an SL membrane after the hydrazine treatment; the hydrazine-treated SL membrane maintains its uniformity over large length scales, up to 1 cm^2 area with no holes or cracks.

For comparison, a similar electron microscopy characterization is performed on a spin-cast PbS GS film before and after hydrazine treatment. Spin-cast PbS GS films typically lead to much thinner films compared to those synthesized by the SL approach. To make a fair comparison, sequential spin-coating deposition steps are employed to produce films with similar thicknesses (140 nm) to the SL membranes (~100 nm, Figure 7b). SEM images in Figure 6c,d show a PbS NC glassy film obtained by our sequential spin-coating technique before (Figure 6c) and after (Figure 6d) hydrazine treatment. The short-range order of the final PbS glassy film is not affected by this chemical process (Figure 6d), and the nonuniform morphology typical of glassy films before hydrazine treatment is retained.[37]

DOI: 10.1021/acsomega.7b00433
ACS Omega 2017, 2, 3681−3690

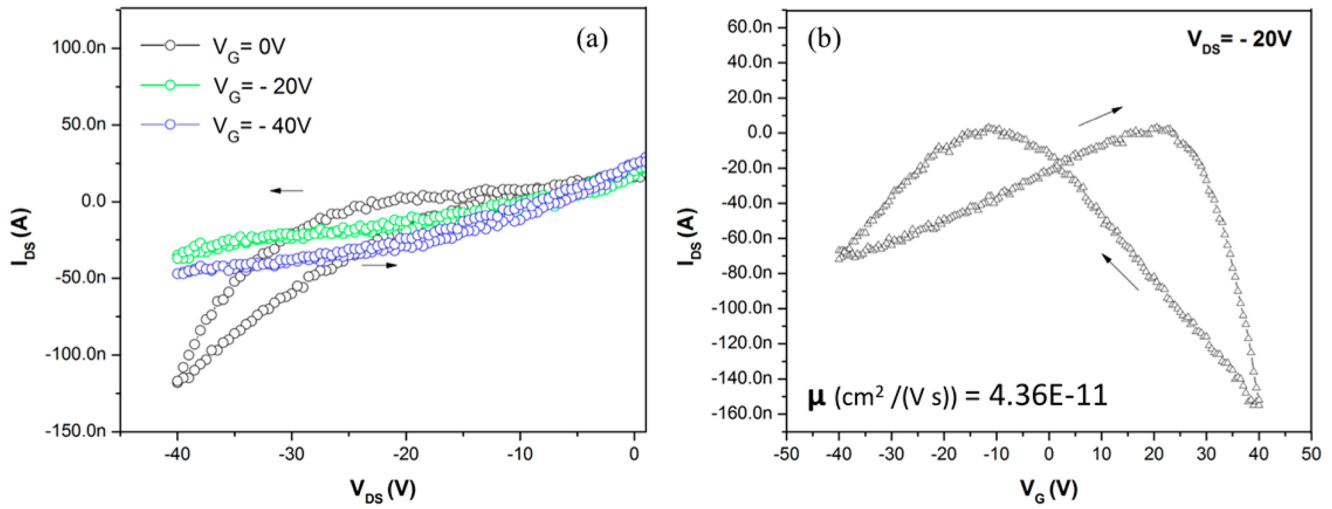

Figure 8. Electrical characterization of a PbS NC spin-cast GS thin film. (a) Typical drain current (I_D)−drain voltage (V_{DS}) characteristics for the bottom-gated thin-film PbS NC GS FET measured at different gate voltages (V_G) in the negative V_D sweep regimes (width and length of the channels were 1 mm and 100 μm, respectively). (b) Transfer curve with a fixed drain−source voltage of −20 V.

Charge-Transport Characterization of PbS SL and GS Films Using an FET Platform. For charge-transport studies, a PbS SL-FET is fabricated by transferring the liquid-supported SL membrane (Results and Discussion) to SiO_2/Si wafer substrates that were prepatterned with source and drain Cr/Au electrodes. Figure 7a shows a schematic cross section of the PbS SL-FET used in this study, where the PbS SL membrane forms a solid-state channel between drain and source contacts. The width (W) and length (L) of the channels were 1 mm and 100 μm, respectively. The as-deposited PbS SL membranes were fairly insulating because of the presence of OA ligands on their surface, which impede charge transport. To enhance electronic coupling between neighboring NCs, postsynthesis hydrazine treatment for 4 h was performed on the PbS SL-FET device. The effect of the hydrazine is to reduce the interparticle spacing between NCs and in turn increase the conductivity of the NC film, as previously reported for PbSe and PbS NC FETs.[33,35]

Figure 7b shows a typical SEM cross section of PbS SL membranes integrated between the drain−source terminals of the FET and exploited for electrical characterization purposes, after hydrazine treatment. The PbS SL on top of the SiO_2 dielectric has a fairly uniform film thickness (t_{SL} = 100 nm) over the whole channel length and width. A thorough electrical characterization of hydrazine-treated SL-FET is performed in a nitrogen atmosphere at RT. In Figure 7, representative output curves I_D−V_{DS} (Figure 7c) and transfer curves I_D−V_{GS} (Figure 7d) of hydrazine-treated SL-FET devices are reported. Figure 7c shows drain current (I_D) versus drain voltage (V_{DS}) scans in the range of 0 to −40 V at various gate voltages (V_G) ranging from 0 to −40 V. SL-FET output curves for drain voltage (V_{DS}) scans in the range of 0 to +40 V are shown in Figure S2a. The absolute current between source and drain electrodes, $|I_D|$, increases linearly with V_{DS} in the range of 0 to −25 V (Figure 7c); however, it tends to saturate on increasing the V_{DS} value over −25 V, as the channel "pinches off" near the drain electrode. An effective modulation of the I_D current flowing through the SL film by application of a negative back-gate voltage is apparent, which is typical of a p-type FET. Figure 7d shows that the absolute value of I_D increases with increasing negative values of V_G at fixed V_{DS} of −20 V, with current modulation ratio (I_{ON}/I_{OFF}) of ∼9. A significant hysteresis over the dynamic range of operation (−40 to +40 V) of V_G is evident in the transfer characteristics of Figure 7d. This effect can be related to the filling of traps associated with dangling bonds on the unpassivated sulfur surface,[38] although this effect has not been investigated in detail in this study. The transfer characteristics apparent in Figure 7d confirms the p-type behavior of the NC SL film with charge accumulation at negative gate voltages. The mobility of the PbS NC FET was estimated from the linear regime.

For comparison, we performed an electrical characterization with similar parameters for the PbS NC GS films obtained by spin casting and treated with hydrazine for 4 h. In a nitrogen glovebox, thin films of NCs were prepared by employing an LbL spin-coating deposition technique using the same oleic acid-passivated PbS NCs used for the SL membranes dispersed in hexane solution on the SiO_2/Si substrate, which was prepatterned with source and drain Cr/Au electrodes. Figure 8a shows typical drain current (I_D)−drain voltage (V_{DS}) characteristics for the bottom-gated PbS GS FET measured at different negative gate voltages (V_G) in the negative V_D sweep regimes. A small increase of the current flowing through the NC film was observed in the V_D range of 0 to −25 V, regardless of the V_G value between 0 and −40 V, with the maximum current value $|I_D|$ = 130 nA at V_G = 0 V. Moreover, at any given V_{DS} value, a small $|I_D|$ modulation is observed on increasing the magnitude of V_G from 0 to −40 V. PbS GS FET output curves for drain voltage (V_{DS}) scans in the range of 0 to +40 V are shown in Figure S2b. To explain the poor electrical behavior of the NC GS films, we refer to the SEM images in Figure 6d, in which one can clearly observe that PbS NC films subjected to 4 h of hydrazine treatment were discontinuous with micron-sized NC aggregates that were not fully connected, thus leaving some portion of the SiO_2 surface free from PbS NCs. The morphology of NC GS films results in poor conductivity. From the transfer characteristics reported in Figure 8b, a low-voltage ambipolar behavior is evident for PbS GS FET with both electron and hole conduction. A switching of the majority carrier is observed from the plot of drain current (I_D) versus gate voltage (V_G) characteristics at fixed values of V_D (e.g., V_D = −20 V), as shown in Figure 8b. Characteristic V-shaped ambipolar curves were obtained, where the right wing (positive V_G) represents electron transport and the left wing (negative V_G) represents hole transport. Some

DOI: 10.1021/acsomega.7b00433
ACS Omega 2017, 2, 3681−3690

hysteresis was evident, which may be explained by carrier trapping. Because of the difference in the current levels for electron and hole conduction, an asymmetry in the V-shape was observed. This arises from differences in the mobility between electrons and holes, as reported in the literature.[14] Similar effects are observed in ethanedithiol-exchanged PbSe NC-based FETs that are moderately conductive and ambipolar in the dark.[39]

For comparison with the PbS SL-FET, we assessed the mobility of PbS GS films and found that it is 3 orders of magnitude lower, with a value of 4.36×10^{-11} cm^2/V s, than that of the PbS SL-FET ($\mu_{SL} = 7.09 \times 10^{-8}$ cm^2/V s).

For electronic devices based on NCs, PbS NC solids combine the advantages of tunable quantum-confined energy levels with fast charge transport owing to the enhanced electronic coupling between NCs that can be improved via controlled ligand exchange. Moreover, assembling hierarchically organized NC solids that display highly periodic patterns over areas spanning square centimeters presents an immense potential for the fabrication of NC-based transistors with enhanced electrical mobility.[40]

CONCLUSIONS

In our study, an NC assembly method is successfully demonstrated as a powerful, lithography-free approach to fabricate large-area NCs assemblies over square centimeter areas that display either short-range (disordered GSs) or long-range (SLs) packing order. We show the dependence of the electronic properties of PbS NCs on their packing order. The long-range ordering arising from the close-packed arrangement of PbS NC SLs leads to higher-conductivity NC solids with respect to PbS NC GSs. In particular, we observe a strong p-type character in PbS NC SL-thin-film-based FETs compared to that in disordered spin-cast films, which show minimal gate modulation. Additionally, SL films show enhanced mobility (greater than 3 orders of magnitude) compared to that of glassy films. In summary, evaporation-mediated self-assembly processes combined with hydrazine treatment has been demonstrated as a promising approach to exert efficient control over particle separation in densely packed 3D SL assemblies of semiconductor NCs over square centimeter areas.

EXPERIMENTAL SECTION

Chemicals. Lead(II) oxide (99.999%), ODE (90%), OA (90%), bis(trimethylsilyl)sulfide (TMS2S), TCE (99%), anhydrous hydrazine (98%), and anhydrous ACN were purchased from Aldrich. Methanol, acetone, hexane, chloroform, ACN, and ethanol were of analytical grade and obtained from various sources. All chemicals were used as received except hydrazine, which was additionally purified by distillation. OA and lead oxide were dried in a Schlenk line for 2 h under vacuum and stored in a nitrogen glovebox.

PbS NC Synthesis. For the synthesis protocol, 0.225 g of PbO, 5 mL of OA, and 5 mL of ODE were loaded in a 25 mL three-neck flask. The mixture was heated to 150 °C under vacuum to form Pb−oleate complex. The synthesis of PbS NCs was followed by the hot-injection method, in which 0.13 mL of TMS2S was dissolved in 2 mL of ODE under stirring. The solution was injected at 100 °C under nitrogen. A rapid nucleation event occurs upon the injection of the S precursor into the Pb−oleate mixture, as evidenced by an immediate color change to brown in the reaction vessel. The reaction mixture was kept at 100 °C under nitrogen for 2−4 min (time growth) and then cooled to RT using a water bath. Key assets of the hot-injection synthesis routine have excellent control over NC size and the narrow size dispersion of resulting colloids. After cooling to RT, the nanoparticles were precipitated from the crude solution by adding a hexane/ethanol (3:1) mixture, followed by centrifugation. Precipitated NCs were redissolved in hexane (~2 mL) and precipitated again with ethanol. PbS NCs were resuspended in octane, hexane, or TCE and used for further preparation and characterization.

Sample Characterization. TEM, powder XRD, and NIR absorption spectroscopy are used to characterize the size, shape, structure, composition, and optical properties of the PbS NCs.

Characterization of particle size, shape, and morphology is carried out via TEM imaging. Samples were prepared by placing 10 μL of a diluted NC solution in toluene or TCE on a 400-mesh carbon-coated copper grid (Ted Pella, Inc.). TEM images were obtained using a JEOL 2100-F 200 kV field-emission analytical transmission electron microscope operating at an acceleration voltage of 120 kV. The particle size and size distribution were calculated on the basis of measurements of at least 100 NCs.

Thin-film characterization is carried out via SEM imaging. Samples were prepared by spin-coating 50 mg/mL PbS solution in hexane on top of an FET device. Top-view images of the NC thin film obtained were acquired using a Zeiss Gemini Ultra-55 analytical field-emission scanning electron microscope operating at 3 kV. The homogeneity and continuity of the PbS NC thin film between the source and drain contacts were analyzed. UV−vis spectroscopy is used to characterize the optical properties of the PbS NCs. For optical absorption measurements, intensively washed (up to three times) NCs were redispersed in TCE. Linear optical absorption spectra were recorded on an ASD QualitySpec Pro UV−vis spectrometer.

Wide-angle powder XRD measurements were carried out on a Bruker AXS D8 Discover GADDS X-ray diffractometer operating in the Bragg−Brentano configuration with Co Kα radiation (λ = 1.54 Å), with scatter and diffraction slits of 1°. Samples for wide-angle XRD measurements are prepared by depositing concentrated PbS NC solutions in hexane onto a silicon surface.

Self-Assembly and Transfer of SL Membranes. In a typical assembly process, 50 mg/mL PbS in octane solution was spread on the ACN solution surface in a Teflon well. The well was covered with a glass slide to slowly control the evaporation of the octane through the gaps between the Teflon surface and the glass slide. Ordered SLs formed upon evaporation of the solvent on top of the liquid−air interface. To transfer PbS SLs, a substrate (e.g., silicon nitride 20 nm floating membrane TEM windows, silicon substrate, SiO_2/Si (100 nm) substrates) was placed under the floating membrane using tweezers and then gently lifted upward to collect the membrane. The subsequent drying in a vacuum chamber removed residual ACN. Close-packed PbS NCs in SL arrangement were treated with hydrazine by dipping the wafers into a 1.0 M solution of hydrazine in anhydrous ACN. The duration of the treatment was 4 h, followed by rinsing the device with anhydrous ACN. The hydrazine-treated NC film is insoluble in common solvents such as hexane and chloroform.

Structural Characterization of PbS SL Membranes. TEM was used to characterize the homogeneity and continuity of PbS NC SL membranes. Samples were prepared by transferring the silicon nitride 20 nm floating membrane TEM windows (Molecular Foundry). TEM images were obtained using a JEOL 2100-F 200 kV field-emission analytical transmission

DOI: 10.1021/acsomega.7b00433
ACS Omega 2017, 2, 3681−3690

electron microscope operating at an acceleration voltage of 120 kV.

Ligand Exchange. The chemical activation process involves treatment of the films with a 1.0 M solution of hydrazine in ACN for 2−5 h and subsequent washing with ACN.

Charge-Transport Characterization. SiO_2/Si (100 nm thick oxide layer) substrates were extensively rinsed with acetone and isopropanol. Then, 5/50 nm deposition was also performed on p-type silicon (back surface) for the gate contact using a shadow mask. The width (W) and length (L) of the channels were 1 mm and 100 μm, respectively. The gate contact was obtained by stretching the SiO_2. Multiple source and drain electrodes were patterned onto a single substrate to allow for electrical measurements using various channel lengths (100 μm).

Drying-mediated self-assembly for SLs and spin-coating deposition for TF of the NC solution were performed on the FET devices.

FET measurements were performed in a glovebox with a homemade probe station using an Agilent 4156B semiconductor parameter analyzer driven by LabVIEW software. The source electrode was grounded. All RT electrical measurements were performed under dry nitrogen atmosphere and in the dark. The electrical properties of PbS SL and PbS glassy thin-film-based transistors were evaluated by a probe station inside a nitrogen glovebox (transistor configuration). The source−drain current (I_{DS}) versus source−drain voltage (V_{DS}) curves under different gate voltages (V_G) of PbS SL-FET and PbS glassy thin-film FET were measured using an Agilent precision semiconductor parameter analyzer.

The source−drain current (I_{DS}) versus gate voltage (V_{GS}) curves biased at a fixed source−drain voltage (V_{DS}) of PbS SL-FET and PbS glassy thin-film FET are measured by a 6487 Picoammeter/Voltage Source (Keithley Instruments), which is used to contemporarily set the voltage (V_{DS}) at −20 V and measure the current (I_{DS}) between the drain and source terminals at different V_{GS} values. A 2400 Source Meter Unit (Keithley Instruments) is used to set the voltage (V_{GS}) at different values. The gate voltage sweep rate was kept constant at 1 V/s throughout the measurement.

The measurement system is PC-controlled using a LabView interface designed to guarantee the correct timing among the different equipment used.

■ ASSOCIATED CONTENT

Supporting Information

The Supporting Information is available free of charge on the ACS Publications website at DOI: 10.1021/acsomega.7b00433.

Morphological analysis of PbS SL membranes (long-range order) and glassy film (short-range order) (Figure S1); electrical characterization of PbS SL and glassy TFs (Figure S2) (PDF)

■ AUTHOR INFORMATION

Corresponding Authors

*E-mail: g.barillaro@iet.unipi.it (G.B.).
*E-mail: jjurban@lbl.gov (J.J.U.).

ORCID

Michela Sainato: 0000-0002-5155-4201
Giuseppe Barillaro: 0000-0001-6197-4851
Jeffrey J. Urban: 0000-0002-6520-830X

Present Addresses

§Electrical and Computer Engineering, University of Illinois at Chicago, 1200 W Harrison Street, 60607 Chicago, United States (M.S.).
∥Chemical and Biomolecular Engineering, NYU Tandon School of Engineering, 6 MetroTech Center, 11201 Brooklyn, United States (A.S.).

Notes

The authors declare no competing financial interest.

■ ACKNOWLEDGMENTS

Work at the Molecular Foundry was supported by Office of Science, Office of Basic Energy Sciences, U.S. Department of Energy, under Contract No. DE-AC02-05CH11231.

■ REFERENCES

(1) Murray, C. B.; Kagan, C. R.; Bawendi, M. G. Synthesis and characterization of monodisperse nanocrystals and close-packed nanocrystal assemblies. *Annu. Rev. Mater. Sci.* **2000**, *30*, 545−610.

(2) Talapin, D. V.; Lee, J. S.; Kovalenko, M. V.; Shevchenko, E. V. Prospects of colloidal nanocrystals for electronic and optoelectronic applications. *Chem. Rev.* **2009**, *110*, 389−458.

(3) De Nolf, K.; Capek, R. K.; Abe, S.; Sluydts, M.; Jang, Y.; Martins, J. C.; Cottenier, S.; Lifshitz, E.; Hens, Z. Controlling the Size of Hot Injection Made Nanocrystals by Manipulating the Diffusion Coefficient of the Solute. *J. Am. Chem. Soc.* **2015**, *137*, 2495−2505.

(4) Wang, J. J.; Liu, P.; Seaton, C. C.; Ryan, K. M. Complete colloidal synthesis of Cu2SnSe3 nanocrystals with crystal phase and shape control. *J. Am. Chem. Soc.* **2014**, *136*, 7954−7960.

(5) Jang, J.; Dolzhnikov, D. S.; Liu, W.; Nam, S.; Shim, M.; Talapin, D. V. Solution-processed transistors using colloidal nanocrystals with composition-matched molecular "solders": approaching single crystal mobility. *Nano Lett.* **2015**, *15*, 6309−6317.

(6) Oh, S. J.; et al. Designing high-performance PbS and PbSe nanocrystal electronic devices through stepwise, post-synthesis, colloidal atomic layer deposition. *Nano Lett.* **2014**, *14*, 1559−1566.

(7) Choi, J.-H.; et al. Bandlike Transport in Strongly Coupled and Doped Quantum Dot Solids: A Route to High-Performance Thin-Film Electronics. *Nano Lett.* **2012**, *12*, 2631−2638.

(8) Talapin, D. V.; Murray, C. B. PbSe nanocrystal solids for n-and p-channel thin film field-effect transistors. *Science* **2005**, *310*, 86−89.

(9) Taleb, A.; Petit, C.; Pileni, M. P. Optical properties of self-assembled 2D and 3D superlattices of silver nanoparticles. *J. Phys. Chem. B* **1998**, *102*, 2214−2220.

(10) Lin, X. M.; Jaeger, H. M.; Sorensen, C. M.; Klabunde, K. J. Formation of long-range-ordered nanocrystal superlattices on silicon nitride substrates. *J. Phys. Chem. B* **2001**, *105*, 3353−3357.

(11) Yang, J.; Wise, F. W. Effects of disorder on electronic properties of nanocrystal assemblies. *J. Phys. Chem. C* **2015**, *119*, 3338−3347.

(12) Gilmore, R. H.; et al. Charge Carrier Hopping Dynamics in Homogeneously Broadened PbS Quantum Dot Solids. *Nano Lett.* **2017**, *17*, 893−901.

(13) Evers, W. H.; et al. High charge mobility in two-dimensional percolative networks of PbSe quantum dots connected by atomic bonds. *Nat. Commun.* **2015**, *6*, No. 8195.

(14) Szendrei, K.; Speirs, M.; Gomulya, W.; Jarzab, D.; Manca, M.; Mikhnenko, O. V.; Yarema, M.; J. Kooi, B.; Heiss, W.; Loi, M. A. Exploring the Origin of the Temperature-Dependent Behavior of PbS Nanocrystal Thin Films and Solar Cells. *Adv. Funct. Mater.* **2012**, *22*, 1598−1605.

(15) Fu, H.; Tsang, S. W. Infrared colloidal lead chalcogenide nanocrystals: synthesis, properties, and photovoltaic applications. *Nanoscale* **2012**, *4*, 2187−2201.

(16) Bisri, S. Z.; Piliego, C.; Yarema, M.; Heiss, W.; Loi, M. A. Low Driving Voltage and High Mobility Ambipolar Field-Effect Transistors with PbS Colloidal Nanocrystals. *Adv. Mater.* **2013**, *25*, 4309−4314.

DOI: 10.1021/acsomega.7b00433
ACS Omega 2017, 2, 3681−3690

(17) Minemawari, H.; Yamada, T.; Matsui, H.; Tsutsumi, J.; Haas, S.; Chiba, R.; Kumai, R.; Hasegawa, T. Inkjet printing of single-crystal films. *Nature* **2011**, *475*, 364−367.
(18) Park, B.; Whitham, K.; Bian, K.; Lim, Y. F.; Hanrath, T. Probing surface states in PbS nanocrystal films using pentacene field effect transistors: controlling carrier concentration and charge transport in pentacene. *Phys. Chem. Chem. Phys.* **2014**, *16*, 25729−25733.
(19) Pileni, M. P. Nanocrystal self-assemblies: fabrication and collective properties. *J. Phys. Chem. B* **2001**, *105*, 3358−3371.
(20) Lee, J. S.; Shevchenko, E. V.; Talapin, D. V. Au−PbS core−shell nanocrystals: Plasmonic absorption enhancement and electrical doping via intra-particle charge transfer. *J. Am. Chem. Soc.* **2008**, *130*, 9673−9675.
(21) de Mello Donegá, C.; Liljeroth, P.; Vanmaekelbergh, D. Physicochemical Evaluation of the Hot-Injection Method, a Synthesis Route for Monodisperse Nanocrystals. *Small* **2005**, *1*, 1152−1162.
(22) Weidman, M. C.; Beck, M. E.; Hoffman, R. S.; Prins, F.; Tisdale, W. A. Monodisperse, air-stable PbS nanocrystals via precursor stoichiometry control. *ACS Nano* **2014**, *8*, 6363−6371.
(23) Moreels, I.; Lambert, K.; Smeets, D.; Muynck, D.; Nollet, T.; Martins, J. C.; Vanhaecke, F.; Vantomme, A.; Delerue, C.; Allan, G.; Hens, Z. Size-dependent optical properties of colloidal PbS quantum dots. *ACS Nano* **2009**, *3*, 3023−3030.
(24) Santhanam, V.; Liu, J.; Agarwal, R.; Andres, R. P. Self-assembly of uniform monolayer arrays of nanoparticles. *Langmuir* **2003**, *19*, 7881−7887.
(25) Brown, J. J.; Porter, J. A.; Daghlian, C. P.; Gibson, U. J. Ordered arrays of amphiphilic gold nanoparticles in Langmuir monolayers. *Langmuir* **2001**, *17*, 7966−7969.
(26) Choi, J. J.; Bealing, C. R.; Bian, K.; Hughes, K. J.; Zhang, W.; Smilgie, D. M.; Hennig, R. G.; Engstrom, J. R.; Hanrath, T. Controlling nanocrystal superlattice symmetry and shape-anisotropic interactions through variable ligand surface coverage. *J. Am. Chem. Soc.* **2011**, *133*, 3131−3138.
(27) Kovalenko, M. V.; Bodnarchuk, M. I.; Talapin, D. V. Nanocrystal superlattices with thermally degradable hybrid inorganic−organic capping ligands. *J. Am. Chem. Soc* **2010**, *132*, 15124−15126.
(28) Schliehe, C.; Juarez, B. H.; Pelletier, M.; Jander, S.; Greshnykh, D.; Nagel, M.; Meyer, A.; Foerster, S.; Kornowski, A.; Klinke, C.; Weller, H. Ultrathin PbS sheets by two-dimensional oriented attachment. *Science* **2010**, *329*, 550−553.
(29) Dong, A.; Chen, J.; Vora, P. M.; Kikkawa, J. M.; Murray, C. B. Binary nanocrystal superlattice membranes self-assembled at the liquid-air interface. *Nature* **2010**, *466*, 474−477.
(30) Dong, A.; Ye, X.; Chen, J.; Murray, C. B. Two-dimensional binary and ternary nanocrystal superlattices: the case of monolayers and bilayers. *Nano Lett.* **2011**, *11*, 1804−1809.
(31) (a) Dong, A.; Chen, J.; Oh, S. J.; Koh, W. K.; Xiu, F.; Ye, X.; Ko, D.; Wang, K. L.; Kagan, C. R.; Murray, C. B. Multiscale periodic assembly of striped nanocrystal superlattice films on a liquid surface. *Nano Lett.* **2011**, *11*, 841−846. (b) Rabani, E.; Reichman, D. R.; Geissler, P. L.; Brus, L. E. Drying-mediated self-assembly of nanoparticles. *Nature* **2003**, *426*, 271−274.
(32) Narayanan, S.; Wang, J.; Lin, X. M. Dynamical self-assembly of nanocrystal superlattices during colloidal droplet evaporation by in situ small angle X-ray scattering. *Phys. Rev. Lett.* **2004**, *93*, No. 135503.
(33) Yu, D.; Wang, C.; Wehrenberg, B. L.; Guyot-Sionnest, P. Variable range hopping conduction in semiconductor nanocrystal solids. *Phys. Rev. Lett.* **2004**, *92*, No. 216802.
(34) Weidman, M. C.; Yager, K. G.; Tisdale, W. A. Interparticle spacing and structural ordering in superlattice PbS nanocrystal solids undergoing ligand exchange. *Chem. Mater.* **2014**, *27*, 474−482.
(35) Berber, M.; Bulto, V.; Kliß, R.; Hahn, H. Transparent nanocrystalline ZnO films prepared by spin coating. *Scr. Mater.* **2005**, *53*, 547−551.
(36) Luther, J. M.; Law, M.; Song, Q.; Perkins, C. L.; Beard, M. C.; Nozik, A. J. Structural, optical, and electrical properties of self-assembled films of PbSe nanocrystals treated with 1, 2-ethanedithiol. *ACS Nano* **2008**, *2*, 271−280.
(37) Fernée, M. J.; Watt, A.; Warner, J.; Cooper, S.; Heckenberg, N.; Rubinsztein-Dunlop, H. Inorganic surface passivation of PbS nanocrystals resulting in strong photoluminescent emission. *Nanotechnology* **2003**, *14*, 991.
(38) Luther, J. M.; Law, M.; Song, Q.; Perkins, C. L.; Beard, M. C.; Nozik, A. J. Structural, optical, and electrical properties of self-assembled films of PbSe nanocrystals treated with 1, 2-ethanedithiol. *ACS Nano* **2008**, *2*, 271−280.
(39) Wang, Y.; Duan, C.; Peng, L.; Liao, J. Dimensionality-dependent charge transport in close-packed nanoparticle arrays: from 2D to 3D 2014. *Sci. Rep.* **2014**, *4*, No. 7565.
(40) Lin, Z.; Wang, M.; Zhang, L.; Xue, Y.; Yao, X.; Cheng, H.; Bai, J. Equilibrium self-assembly of close-packed ordered PbTe nanocrystal thin film and near-infrared photoconductive detector. *J. Mater. Chem.* **2012**, *22*, 9082−9085.

DOI: 10.1021/acsomega.7b00433
ACS Omega 2017, 2, 3681−3690